Commun. Comput. Phys.
doi: 10.4208/cicp.250111.210611a

Vol. **12**, No. 1, pp. 226-246
July 2012

Fast Multipole Accelerated Boundary Integral Equation Method for Evaluating the Stress Field Associated with Dislocations in a Finite Medium

Degang Zhao[1,2], Jingfang Huang[3] and Yang Xiang[4,*]

[1] *Nano Science and Technology Program, The Hong Kong University of Science and Technology, Clear Water Bay, Kowloon, Hong Kong.*
[2] *School of Physics, Huazhong University of Science and Technology, Wuhan 430074, China.*
[3] *Department of Mathematics, The University of North Carolina at Chapel Hill, Chapel Hill, NC 27599-3250, USA.*
[4] *Department of Mathematics, The Hong Kong University of Science and Technology, Clear Water Bay, Kowloon, Hong Kong.*

Received 25 January 2011; Accepted (in revised version) 21 June 2011

Communicated by Wei Cai

Available online 27 January 2012

Abstract. In this paper, we develop an efficient numerical method based on the boundary integral equation formulation and new version of fast multipole method to solve the boundary value problem for the stress field associated with dislocations in a finite medium. Numerical examples are presented to examine the influence from material boundaries on dislocations.

AMS subject classifications: 74S15, 65R20, 74A10, 74B05

Key words: Fast multipole method, boundary integral equation method, dislocation dynamics, stress.

1 Introduction

The collective motion and interaction of large numbers of dislocations (line defects) play central roles in the plastic deformation of crystals [1]. The direct numerical simulation of interaction and motion of dislocations, known as dislocation dynamics, is becoming a more and more important tool for the investigation of the plastic properties of crystalline materials [2–26]. However, in order for dislocation dynamics to be a practical engineering tool, large ensembles of dislocations are required in the simulations, which are still beyond the capability of currently available dislocation dynamics methods.

*Corresponding author. *Email addresses:* dgzhao@mail.hust.edu.cn (D. G. Zhao), huang@amath.unc.edu (J. F. Huang), maxiang@ust.hk (Y. Xiang)

One of the major limitations of the current dislocation dynamics methods lies in the computational cost for the complex, long-range elastic interactions of dislocations that depend on the relative positions of dislocations, their orientations as well as their Burgers vectors. When a direct method is applied to find the summation of interactions between dislocation segments in numerical discretization of dislocations, the calculation is inherently time consuming and requires $\mathcal{O}(N^2)$ operations, where N is the total number of dislocation segments. Employing cut-off distance is known to produce spurious results [2,4]. Several fast numerical algorithms for the long-range interaction of dislocations in dislocation dynamics simulations have been introduced to reduce the computational cost to achieve the asymptotically optimal $\mathcal{O}(N)$ efficiency [4, 6, 11, 17, 21, 23, 26]. Previously in [26], we have applied the new version of fast multipole method (FMM) [27] to compute the stress field of dislocation ensembles in an infinite medium. Numerical experiments showed that for a dislocation ensemble discretized into N dislocation segments, the new version FMM based method is asymptotically $\mathcal{O}(N)$ with an optimized prefactor and is very efficient for prescribed accuracy requirements.

For materials with boundaries such as thin film materials, there are interactions between dislocations and material boundaries, resulting in image forces on dislocations. Analytical formulas for the image forces are only available for some special cases, e.g., some straight dislocations in half space with a planar free surface [1]. Generally, a complementary stress field should be obtained to satisfy the given boundary conditions, e.g., the traction free boundary conditions [28]. The superposition of the (a) stress field associated with the dislocations in an infinite elastic medium and (b) stress field obtained from solving the boundary value problem without dislocations gives the correct stress field in the finite medium containing dislocations. In most existing simulations, the complementary problem is solved by the finite element method (FEM) [10,12,14,22]. For the special cases of a half space with a planar free surface, Green's function method or FFT are used to solve the boundary value problem [5,7,18,19]; and there are also techniques to include the image forces based on prismatic loops [13,16].

The boundary integral equation method (BIEM) [29] (also called the boundary element method) was developed shortly after the introduction of the finite element methods (FEM) in the 1950s. Compared with the volume discretization in the FEM, BIEM only requires the discretization of the surface and the number of unknowns and required memory are therefore much less than those in the FEM. When applied to dislocation dynamics, once the information on the surface is solved, BIEM is able to evaluate the driving force on dislocations accurately at any point inside the medium, whereas in the FEM, interpolation is needed from the values on the prescribed numerical grid points in the volume discretization. However, as the matrix of the resulting linear system in BIEM is dense, for a problem with N unknowns, when Gauss elimination is applied, $\mathcal{O}(N^3)$ operations and $\mathcal{O}(N^2)$ memory are required. The huge computational cost and storage requirement quickly exhaust the computer resources when $N>10^4$ and the BIEM was less competitive compared with the multigrid and/or domain decomposition accelerated FEM. In the last twenty years or so, to break this bottleneck, by observing the special structure of the ma-

trices, the FMM was coupled with the Krylov subspace type methods to efficiently solve the BIEM formulations [30–36]. When a well-conditioned boundary integral equation is used, the fast BIEM only requires $\mathcal{O}(N)$ or $\mathcal{O}(N\log N)$ operations and memory storage. Although BIEM has been employed in dislocation dynamics problems [24], these advanced numerical techniques were not used.

In this paper, we develop an efficient numerical method based on the boundary integral equation formulation accelerated by FMM to solve for the image stress field associated with dislocations in a finite medium. The resulting discretized linear system is then solved efficiently by the Krylov subspace methods and each matrix vector multiplication is accelerated by the new version of fast multipole method. This fast BIEM can be coupled with the efficient numerical method for the stress field of dislocation ensembles in an infinite medium presented in [26]. Numerical examples are presented to examine the influence from material boundaries on dislocations.

2 Continuum theory of dislocations

In this section, we briefly review the continuum theory of dislocations [1].

In the continuum theory, within the medium containing the dislocations, the elastic displacement vector $\mathbf{u}=(u_1,u_2,u_3)$ is increased by the amount of its Burgers vector $\mathbf{b}=(b_1,b_2,b_3)$ along any loop enclosing the dislocation:

$$\oint_L \frac{\partial \mathbf{u}}{\partial l} dl = \mathbf{b}, \tag{2.1}$$

where L is any contour enclosing the dislocation line and $\partial\mathbf{u}/\partial l$ is the elastic displacement gradient along the contour.

In the linear elasticity theory, the strain tensor is defined as

$$\varepsilon_{ij} = \frac{1}{2}\Big(\frac{\partial u_i}{\partial x_j} + \frac{\partial u_j}{\partial x_i}\Big), \tag{2.2}$$

for $i,j=1,2,3$. the stress tensor σ is determined from the strain tensor by the linear elastic constitutive equations (Hooke's law):

$$\sigma_{ij} = \sum_{k,l=1,2,3} C_{ijkl}\varepsilon_{kl}, \tag{2.3}$$

for $i,j=1,2,3$, where $\{C_{ijkl}\}$ is the elastic constant tensor. In an isotropic medium, the constitutive equations are

$$\sigma_{11} = \frac{2\mu}{1-2\nu}[(1-\nu)\varepsilon_{11}+\nu\varepsilon_{22}+\nu\varepsilon_{33}], \qquad \sigma_{12}=\sigma_{21}=2\mu\varepsilon_{12}, \tag{2.4a}$$

$$\sigma_{22} = \frac{2\mu}{1-2\nu}[\nu\varepsilon_{11}+(1-\nu)\varepsilon_{22}+\nu\varepsilon_{33}], \qquad \sigma_{23}=\sigma_{32}=2\mu\varepsilon_{23}, \tag{2.4b}$$

$$\sigma_{33} = \frac{2\mu}{1-2\nu}[\nu\varepsilon_{11}+\nu\varepsilon_{22}+(1-\nu)\varepsilon_{33}], \qquad \sigma_{31}=\sigma_{13}=2\mu\varepsilon_{31}, \tag{2.4c}$$

where μ is the shear modulus and ν is the Poisson's ratio. The stress tensor satisfies equilibrium equations. In the absence of body forces, the equilibrium equations are

$$\nabla\cdot\sigma=0. \tag{2.5}$$

In an infinite isotropic medium, the analytical expression of the stress tensor due to a dislocation loop is a line integral along the dislocation given by [1]

$$\sigma_{ij}(\mathbf{X})=\sum_{m,n,k,p=1,2,3}\frac{\mu b_n}{8\pi}\oint_c\left[R_{,mpp}(\varepsilon_{jmn}dl_i+\varepsilon_{imn}dl_j)+\frac{2}{1-\nu}\varepsilon_{kmn}(R_{,ijm}-\delta_{ij}R_{,ppm})dl_k\right], \tag{2.6}$$

where c is the dislocation loop, (dl_1,dl_2,dl_3) is the line element along the dislocation, $\mathbf{X}=(x_1,x_2,x_3)$ is the target point, $\mathbf{Y}=(y_1,y_2,y_3)$ is a source point on the dislocation loop,

$$R=\sqrt{(x_1-y_1)^2+(x_2-y_2)^2+(x_3-y_3)^2}$$

is the distance between $\mathbf{X}$ and $\mathbf{Y}$, $R_{,ijk}$ is the third order partial derivative of R with respect to spatial variables defined as $R_{,ijk}=\partial^3R/\partial x_i\partial x_j\partial x_k$, δ_{ij} is the Kronecker tensor, which is 1 when $i=j$ and 0 otherwise, ε_{ijk} is the permutation tensor, which is 1 when $ijk=123$, 231, 312, -1 when $ijk=132$, 213, 321, and 0 otherwise, and the summations are taken for repeated indices.

The elastic strain energy stored in the medium is

$$W=\int\sum_{i,j=1,2,3}\frac{1}{2}\sigma_{ij}\varepsilon_{ij}dV. \tag{2.7}$$

The force acting on the dislocation, referred to as the Peach-Koehler force [37], can be obtained by taking variation of this energy with respect to the position of the dislocation

$$\mathbf{F}=\sigma\cdot\mathbf{b}\times\xi, \tag{2.8}$$

where ξ is the unit tangent vector of the dislocation. At low velocities, the motion of dislocations can be thought of as purely dissipative and the dislocation velocity can be written as

$$\mathbf{v}=\mathbf{M}\cdot\mathbf{F}, \tag{2.9}$$

where $\mathbf{M}$ is the dislocation mobility tensor. This velocity formula is commonly used in dislocation dynamics simulations [2–26].

For the boundary conditions of an elasticity problem in a finite medium, displacement vector $\mathbf{u}$ is given on part of the boundary and the traction $\mathbf{T}=\sigma\cdot\mathbf{n}$ is specified on the other part of the boundary. In this paper, we focus on the calculation of the stress field in a finite medium. In dislocation dynamics simulations in a finite medium, a widely used boundary condition is the traction-free boundary condition, i.e., the traction

$$\mathbf{T}=0,\quad \text{on the material boundary}, \tag{2.10}$$

where $\mathbf{n}$ is the unit outer normal vector of the material boundary.

3 Boundary integral equation method

In this section, we briefly review the boundary integral equation method (BIEM) for the elasticity system of Eqs. (2.2), (2.3) and (2.5) (without dislocations) [29].

3.1 BIEM for elasticity system

For an elasticity system without body force, the boundary integral equations for the elasticity system of Eqs. (2.2), (2.3) and (2.5) are

$$\frac{1}{2}u_i(\mathbf{x})+\int_S\sum_{j=1}^{3}T_{ij}(\mathbf{x},\mathbf{y})u_j(\mathbf{y})dS_y=\int_S\sum_{j=1}^{3}U_{ij}(\mathbf{x},\mathbf{y})t_j(\mathbf{y})dS_y, \tag{3.1}$$

for $i=1,2,3$, where S is the boundary of the medium, $\mathbf{x}=(x_1,x_2,x_3)$, $\mathbf{y}=(y_1,y_2,y_3)$ are the spatial coordinates of the boundary, $\mathbf{T}=(t_1,t_2,t_3)$ is the traction on the surface and functions $U_{ij}(\mathbf{x},\mathbf{y})$ and $T_{ij}(\mathbf{x},\mathbf{y})$ are the Green's functions. In an isotropic medium, the constitutive equations are given by Eq. (2.4) and the Green's functions are

$$U_{ij}(\mathbf{x},\mathbf{y})=\frac{1}{16\pi\mu(1-\nu)R}\left[(3-4\nu)\delta_{ij}+\frac{(x_i-y_i)(x_j-y_j)}{R^2}\right], \tag{3.2a}$$

$$T_{ij}(\mathbf{x},\mathbf{y})=\frac{1}{8\pi(1-\nu)R^2}\left[(1-2\nu)\left(\frac{(x_j-y_j)n_i(\mathbf{y})}{R}-\frac{(x_i-y_i)n_j(\mathbf{y})}{R}\right)\right.$$
$$\left.-\frac{\partial R}{\partial n}\left((1-2\nu)\delta_{ij}+3\frac{(x_i-y_i)(x_j-y_j)}{R^2}\right)\right], \tag{3.2b}$$

where $R=|\mathbf{x}-\mathbf{y}|$ is the distance between two points $\mathbf{x}$ and $\mathbf{y}$, δ_{ij} equals 1 when $i=j$ and 0 otherwise, $\mathbf{n}=(n_1,n_2,n_3)$ is the outer normal vector of the surface and $\partial R/\partial n$ is the partial derivative of R in the outer normal direction. Recall that in the boundary conditions, displacement vector $\mathbf{u}=(u_1,u_2,u_3)$ is given on part of the boundary S and the traction $\mathbf{T}=(t_1,t_2,t_3)$ is given on the other part of S. The displacement and traction on the boundary that are not specified in the boundary conditions can be solved from these boundary integral equations in Eq. (3.1). Once these integral equations are solved, the displacement at any point $\mathbf{x}'$ inside the medium can be obtained by

$$u_i(\mathbf{x}')=\int_S\sum_{j=1}^{3}U_{ij}(\mathbf{x}',\mathbf{y})t_j(\mathbf{y})dS_y-\int_S\sum_{j=1}^{3}T_{ij}(\mathbf{x}',\mathbf{y})u_j(\mathbf{y})dS_y, \tag{3.3}$$

for $i=1,2,3$.

Numerically, by standard finite element discretization techniques, the integral equations in Eq. (3.1) can be converted into algebraic equations. For the discretization types, there are constant elements, linear elements, quadratic elements and higher order elements. In the numerical implementation in this paper, we adopt the constant element

approximation except in the element containing the target point over which the integrals in Eq. (3.1) are singular and linear approximations are used, see Appendix. More precisely, we divide the boundary S into N elements and for each element, the spatial coordinates of its center is defined as its location. Then we can obtain at each boundary element location $\mathbf{y}_{k_0}$ the discrete boundary integral equations

$$\begin{aligned}&\frac{1}{2}u_i(\mathbf{y}_{k_0})+\sum_{j=1}^{3}\sum_{k\neq k_0}^{N}T_{ij}(\mathbf{y}_{k_0},\mathbf{y}_k)S_k u_j(\mathbf{y}_k)+L_{u_i}\big(\mathbf{u}(\mathbf{y}_{k_0}),\triangle\mathbf{u}(\mathbf{y}_{k_0})\big)\\&=\sum_{j=1}^{3}\sum_{k\neq k_0}^{N}U_{ij}(\mathbf{y}_{k_0},\mathbf{y}_k)S_k t_j(\mathbf{y}_k)+L_{t_i}\big(\mathbf{T}(\mathbf{y}_{k_0}),\triangle\mathbf{T}(\mathbf{y}_{k_0})\big),\end{aligned}\tag{3.4}$$

for $i=1,2,3$, where S_k is the area of the k-th boundary element, $L_{u_i}(\mathbf{u}(\mathbf{y}_{k_0}),\triangle\mathbf{u}(\mathbf{y}_{k_0}))$ $(L_{t_i}(\mathbf{T}(\mathbf{y}_{k_0}),\triangle\mathbf{T}(\mathbf{y}_{k_0})))$ are linear functions of $\mathbf{u}(\mathbf{y}_{k_0})$ $(\mathbf{T}(\mathbf{y}_{k_0}))$ and its first partial derivatives approximated by some finite difference expressions denoted by $\triangle\mathbf{u}(\mathbf{y}_{k_0})$ $(\triangle\mathbf{T}(\mathbf{y}_{k_0}))$. The terms of $L_{u_i}(\mathbf{u}(\mathbf{y}_{k_0}),\triangle\mathbf{u}(\mathbf{y}_{k_0}))$ and $L_{t_i}(\mathbf{T}(\mathbf{y}_{k_0}),\triangle\mathbf{T}(\mathbf{y}_{k_0}))$ come from the singular integrals over the boundary element containing the target point $\mathbf{y}_{k_0}$ itself and the detailed expressions of them are calculated in Appendix. The solution method for this algebraic system will be discussed in the next subsection.

After solving the above algebraic system for the unspecified $\mathbf{u}=(u_1,u_2,u_3)$ and $\mathbf{T}=(t_1,t_2,t_3)$ on S in the boundary conditions, the displacement at any point $\mathbf{x}'$ inside the medium can be obtained using the displacement and traction on the boundary from a discretized form of Eq. (3.3):

$$u_i(\mathbf{x}')=\sum_{j=1}^{3}\sum_{k=1}^{N}U_{ij}(\mathbf{x}',\mathbf{y}_k)t_j(\mathbf{y}_k)S_k-\sum_{j=1}^{3}\sum_{k=1}^{N}T_{ij}(\mathbf{x}',\mathbf{y}_k)u_j(\mathbf{y}_k)S_k,\tag{3.5}$$

for $i=1,2,3$.

Note that in Eq. (3.4), the physical parameters (u_1,u_2,u_3) and (t_1,t_2,t_3) are used in the Green's second identity based formulation (sometimes referred to as the natural boundary integral equation formulation). An alternative approach is to represent the solution as combinations of different layer potentials with non-physical unknown density functions, and develop a well-conditioned Fredholm second kind boundary integral equation formulation. When the Krylov subspace methods are applied to such well-conditioned systems, the number of iterations will be independent of the number of unknowns, making it possible to develop asymptotically optimal $\mathcal{O}(N)$ algorithms. We are currently searching for such Fredholm second kind formulations and results will be presented in the future.

3.2 Krylov subspace methods

Moving all unknowns in Eq. (3.4) to the left and all known quantities to the right, one obtains a general linear system

$$\mathbf{A}\boldsymbol{x}=\mathbf{B}.\tag{3.6}$$

Assuming there are N unknowns, when the LU decomposition based Gauss elimination (GE) is applied to the dense linear system, $\mathcal{O}(N^2)$ memory and $\mathcal{O}(N^3)$ operations are required, which is not effective for large N. Alternatively, one can apply the least square based Krylov subspace methods to iteratively search for the optimal solution in the corresponding Krylov subspace. As our linear system is in general non-symmetric and there exist no fast algorithms for computing the product of A^T with a given vector, applicable Krylov subspace methods include the generalized minimal residual (GMRES), biconjugate gradients stabilized (BiCGStab) and transpose-free quasi-minimal residual (TFQMR) algorithms (see [38] for detailed discussions of the Krylov subspace methods), which have been widely used to solve boundary integral equations [38–43]. Our preliminary numerical experiments show that the GMRES method converges faster than other methods, which agrees with existing analyses. However, as the memory required by the GMRES method increases linearly with the iteration number k and the number of multiplications scales like $\frac{1}{2}k^2N$, for large k, the GMRES procedure may become very expensive and requires excessive memory storage. For these reasons, instead of a full orthogonalization procedure, GMRES can be restarted every k_0 steps where $k_0 < N$ is some fixed integer parameter. The restarted version is often denoted as GMRES(k_0). In the following, we briefly describe the GMRES(k_0) algorithm used in our current implementation.

1. *Start*: Choose initial vector $\mathbf{X}_0$ and compute $\mathbf{r}_0 = \mathbf{B} - \mathbf{A}\mathbf{X}_0$. Let $\beta = \|\mathbf{r}_0\|$, $\mathbf{v}_1 = \mathbf{r}_0/\beta$. Set the error tolerance to ε.

2. *Iterate*: For $j = 1,2,\cdots,k_0$ do:

$$h_{i,j} = (\mathbf{A}\cdot\mathbf{v}_j, \mathbf{v}_i), \quad i = 1,2,\cdots,j, \qquad \widehat{\mathbf{v}}_{j+1} = \mathbf{A}\cdot\mathbf{v}_j - \sum_{i=1}^{j} h_{i,j}\cdot\mathbf{v}_i,$$
$$h_{j+1,j} = \|\widehat{\mathbf{v}}_{j+1}\|, \qquad \mathbf{v}_{j+1} = \widehat{\mathbf{v}}_{j+1}/h_{j+1,j}.$$

   Form $\overline{H}_{k_0}$ using computed $h_{i,j}$.

3. *Form approximate solution*:

$$\mathbf{X}_{k_0} = \mathbf{X}_0 + \mathbf{V}_{k_0}\mathbf{Y},$$

   where $\mathbf{Y}$ minimizes $\|\beta\mathbf{e}_1 - \overline{H}_{k_0}\mathbf{Y}\|$, $\mathbf{e}_1 = (1,0,0,\cdots)^T$, $\mathbf{V}_{k_0} = (\mathbf{v}_1, \mathbf{v}_2, \cdots, \mathbf{v}_{k_0})$.

4. *Restart*: Compute

$$\mathbf{r}_{k_0} = \mathbf{B} - \mathbf{A}\mathbf{X}_{k_0},$$

   if $\|\mathbf{r}_{k_0}\|/\beta < \varepsilon$, then stop; else let $\mathbf{X}_0 = \mathbf{X}_{k_0}$, $\mathbf{v}_1 = \mathbf{r}_{k_0}/\|\mathbf{r}_{k_0}\|$ and go to Step 2.

In addition to the GMRES(k_0), we have also tested BiCGStab and TFQMR, our numerical results show very similar convergence rates and the numbers of iterations increase only slightly when compared with the original GMRES procedure. However for large number of Krylov iterations, the required memory is bounded and the number of multiplications only grows linearly in the GMRES(k_0), BiCGStab and TFQMR algorithms.

4 FMM accelerated BIEM for elasticity system associated with dislocations

To obtain the elasticity fields associated with dislocations in a finite medium, Van der Giessen and Needleman [28] introduced a general method for the incorporation of boundary conditions. In particular, an elastic field of dislocations in finite medium is the superposition of (a) the elastic field associated with dislocations in an infinite elastic medium and (b) the elastic field obtained from a complementary boundary value problem without dislocations to satisfy the given boundary conditions, i.e.,

$$u_i = \tilde{u}_i + \hat{u}_i, \qquad \epsilon_{ij} = \tilde{\epsilon}_{ij} + \hat{\epsilon}_{ij}, \qquad \sigma_{ij} = \tilde{\sigma}_{ij} + \hat{\sigma}_{ij}, \tag{4.1}$$

where the $\tilde{(\cdot)}$ fields are generated by dislocations in an infinite medium and the $\hat{(\cdot)}$ fields are those from the complementary problem in order to satisfy the boundary conditions. Fig. 1 illustrates this decomposition approach.

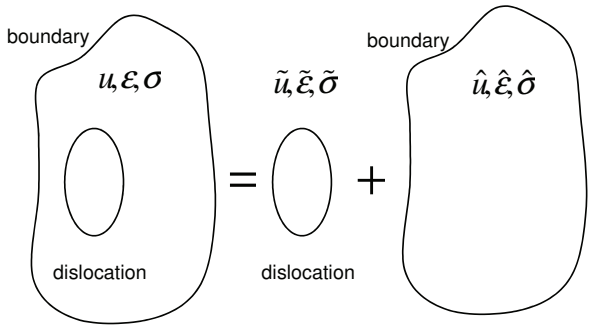

Figure 1: Decomposition of elastic fields associated with dislocations in a finite medium.

The $\tilde{(\cdot)}$ fields generated by dislocations in an infinite medium have integral formulas [1]. For dislocations in an infinite isotropic medium, the stress field is given by Eq. (2.6). Direct numerical calculation of the integrals in Eq. (2.6) requires $\mathcal{O}(N^2)$ operations, where N is the total number of dislocation segments in the discretization. In our method, this stress field is calculated efficiently using the new version of FMM as presented in [26], which is asymptotically $\mathcal{O}(N)$ efficiency with an optimized prefactor.

We solve the complementary $\hat{(\cdot)}$ fields in the finite medium within the framework of BIEM. In this paper, we focus on the traction free boundary condition, see Eq. (2.10). The $\tilde{(\cdot)}$ fields generated by dislocations in an infinite medium obtained above generally do not satisfy this boundary condition. In the complementary problem, no dislocations are contained inside the medium and the traction-free boundary condition is satisfied by adding on the boundary a negative traction from the $\tilde{(\cdot)}$ fields in an infinite medium obtained above, i.e., $\hat{t}_i = -\tilde{t}_i = -\sum_{j=1}^{3} \tilde{\sigma}_{ij} n_j$. The BIEM formulation is given in Eq. (3.1), in which the traction $\mathbf{T} = (t_1, t_2, t_3)$ is given everywhere on the boundary and the unknown functions

are the displacement vector $\mathbf{u}=(u_1,u_2,u_3)$ on the boundary. For the discretization of these boundary integral equations, we use the formulation in Eq. (3.4), which is a linear system of $\{u_i(\mathbf{y}_k)\}$, $i=1,2,3$.

The resulting linear system in Eq. (3.4) is solved iteratively using the restarted GMRES algorithm described in Section 3.2. In the iterations, the matrix-vector products are calculated efficiently using the new version FMM. This reduces both the operation count and memory from $\mathcal{O}(N^2)$ to the asymptotically optimal $\mathcal{O}(N)$ for each Krylov iteration step, where N is the total number of unknowns in the BIEM discretization. Note that for the dense linear system, the Krylov subspace methods do not require the storage of each entry in the matrix, but only the results of the matrix vector multiplication computed using the new version of FMM. In our current FMM implementation, by representing the Green's functions $U_{ij}(\mathbf{x},\mathbf{y})$ and $T_{ij}(\mathbf{x},\mathbf{y})$ as different partial derivatives of the harmonic kernel as

$$U_{ij}(\mathbf{x},\mathbf{y})=\frac{1}{16\pi\mu(1-\nu)}\left[(3-4\nu)\delta_{ij}-x_j\frac{\partial}{\partial x_i}\right]\frac{1}{R}+\frac{1}{16\pi\mu(1-\nu)}\frac{\partial}{\partial x_i}\left(\frac{y_j}{R}\right), \tag{4.2a}$$

$$\begin{aligned}T_{ij}(\mathbf{x},\mathbf{y})=&\frac{1-2\nu}{8\pi(1-\nu)}\left[\frac{\partial}{\partial x_i}\left(\frac{n_j(\mathbf{y})}{R}\right)-\frac{\partial}{\partial x_j}\left(\frac{n_i(\mathbf{y})}{R}\right)-\delta_{ij}\sum_{s=1}^{3}\frac{\partial}{\partial x_s}\left(\frac{n_s(\mathbf{y})}{R}\right)\right]\\&+\frac{1}{8\pi(1-\nu)}\left[\sum_{s=1}^{3}x_s\frac{\partial^2}{\partial x_i\partial x_j}\left(\frac{n_s(\mathbf{y})}{R}\right)-\sum_{s=1}^{3}\frac{\partial^2}{\partial x_i\partial x_j}\left(\frac{y_s n_s(\mathbf{y})}{R}\right)\right],\end{aligned} \tag{4.2b}$$

for all $i,j=1,2,3$, we utilize existing new version of FMM package *FMMSuite* developed by one of the authors from [44]. Interested readers are referred to [27,45] for details of the new version of FMM. In our current implementation, 6 harmonic FMMs are used to calculate the summations $\sum_{k\neq k_0}^{N}\sum_{j=1}^{3}U_{ij}(\mathbf{x},\mathbf{y}_k)t_j(\mathbf{y}_k)S_k$, and 12 for $\sum_{k\neq k_0}^{N}\sum_{j=1}^{3}T_{ij}(\mathbf{x},\mathbf{y}_k)u_j(\mathbf{y}_k)S_k$ in Eq. (3.4). Therefore a total of 18 harmonic FMMs are needed in each Krylov iteration. We are currently investigating possible strategies to further reduce this number.

Once the numerical values of the displacement vector on the boundary are obtained, the displacement at any point inside the medium can be evaluated conveniently using Eq. (3.5). One advantage of the BIEM formulation over FEM is that given the numerical values on the boundary, the elastic fields inside the medium can be evaluated accurately using BIEM, whereas in the FEM formulation, interpolations are generally needed except when the locations where these fields are evaluated are the same as the nodal points. This advantage is crucial in dislocation dynamics simulations, in which the elastic fields are evaluated on dislocations which move continuously inside the medium.

In this paper, we focus on the calculation of the stress field associated with dislocations in a finite medium, which determines the velocity of dislocations and is a crucial step in dislocation dynamics simulations. We calculate the stress tensor from the displacement vector given by Eq. (3.5) using difference approximations. A convergence test of this difference approximation scheme is given in Fig. 5 in the next section.

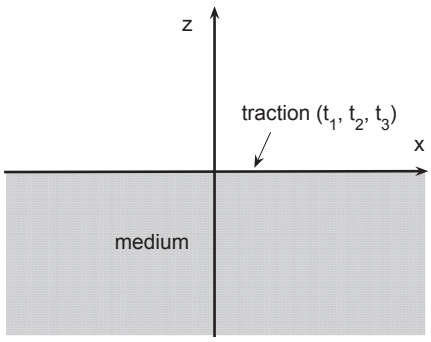

Figure 2: A half space medium.

5 Numerical results

In this section, we present some numerical examples using our method.

In the first numerical example, we examine the accuracy of our method for solving the boundary value problem of the elasticity system. For the purpose of comparison, we choose a special case where analytical solution is available. We consider a half-space medium $z \leq 0$, see Fig. 2. The boundary of this medium is the xy plane, on which the traction is:

$$t_1 = t_2 = 0, \qquad t_3 = \cos 2\pi x. \tag{5.1}$$

Under this boundary condition, the displacement has explicit solution (e.g., [46], Appendix N). The components of the displacement vector on the surface are:

$$u_1 = \frac{1-2\nu}{4\pi\mu}\sin 2\pi x, \qquad u_2 = 0, \qquad u_3 = \frac{1-\nu}{2\pi\mu}\cos 2\pi x. \tag{5.2}$$

We choose the computational domain for the boundary to be $[-1,1]^2$. As most of the existing open source FMM solvers only consider the so called "free space" kernels and do not apply directly to periodic problems, we include 5 replica of the domain in the x direction (no need to repeat the cell in the y direction along which the solution is uniform). We then consider the solution for $x \in [-0.5,0.5]$ and $y = 0$, for which the cut-off effect is small. We want to mention that currently the *FMMSuite* is being upgraded to allow periodic and other boundary conditions and the open source code will be released in the future.

Fig. 3 shows the numerical results and comparisons with the analytical formula for the displacement on the boundary. The boundary $[-1,1]^2$ is discretized into rectangular meshes using grid sizes $\Delta x = \Delta y = 0.01$. The number of expansion terms in the FMM is $p = 9$ for 3 digits accuracy [26]. The figure shows excellent agreement between our numerical results and those from analytical formula and the maximum relative error is about 0.9%.

In the second example, we consider a circular prismatic dislocation loop located at the center of a $L \times L \times L/2$ cuboid box as shown in Fig. 4. The Burgers vector **b** is in the

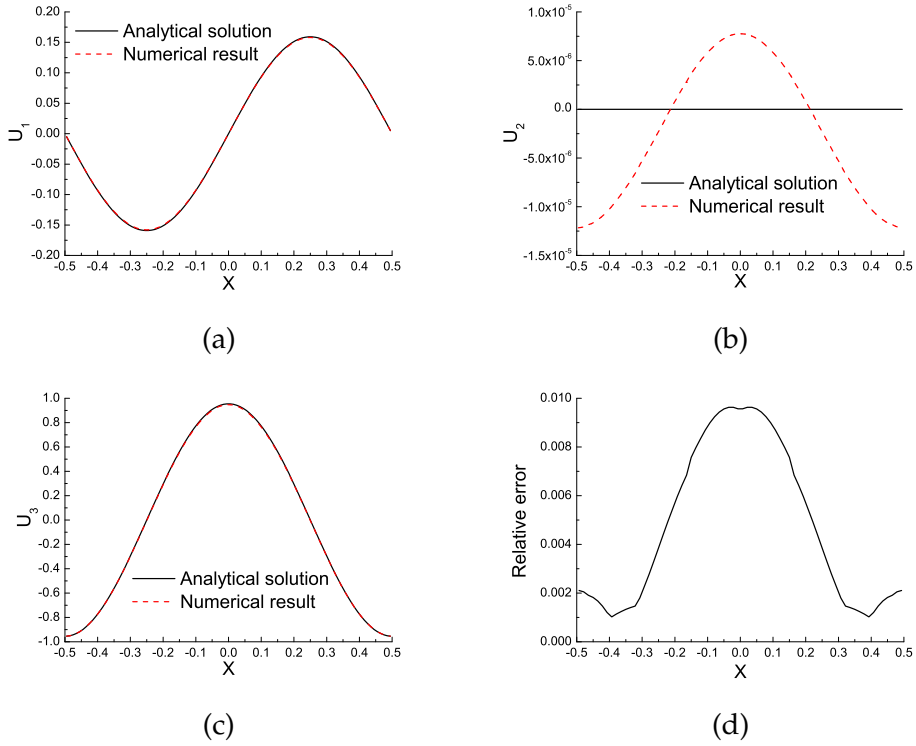

Figure 3: Comparison of our numerical results with the analytical formulas for the displacement vector $\mathbf{u}=(u_1,u_2,u_3)$ on the boundary of the half space medium. The l^∞ norm of vector $\mathbf{u}$ is used in (d).

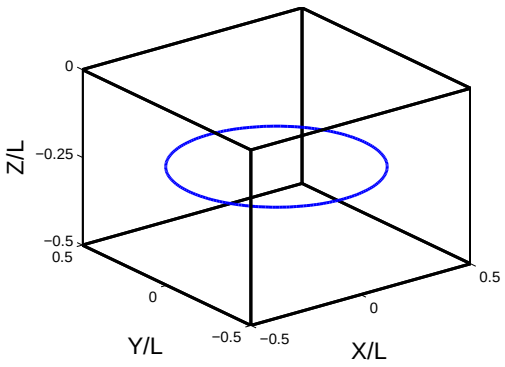

Figure 4: A prismatic dislocation loop in a cuboid box.

z direction and the radius of dislocation loop is $r=0.4L=200b$, where b is the length of the Burgers vector. Traction-free boundary conditions are used for the whole boundary. Rectangular mesh is used in the boundary discretization with $\Delta x=\Delta y=\Delta z$.

We first present convergence tests for the stress calculation. As described in the previous section, after the boundary integral equations are solved, we use difference ap-

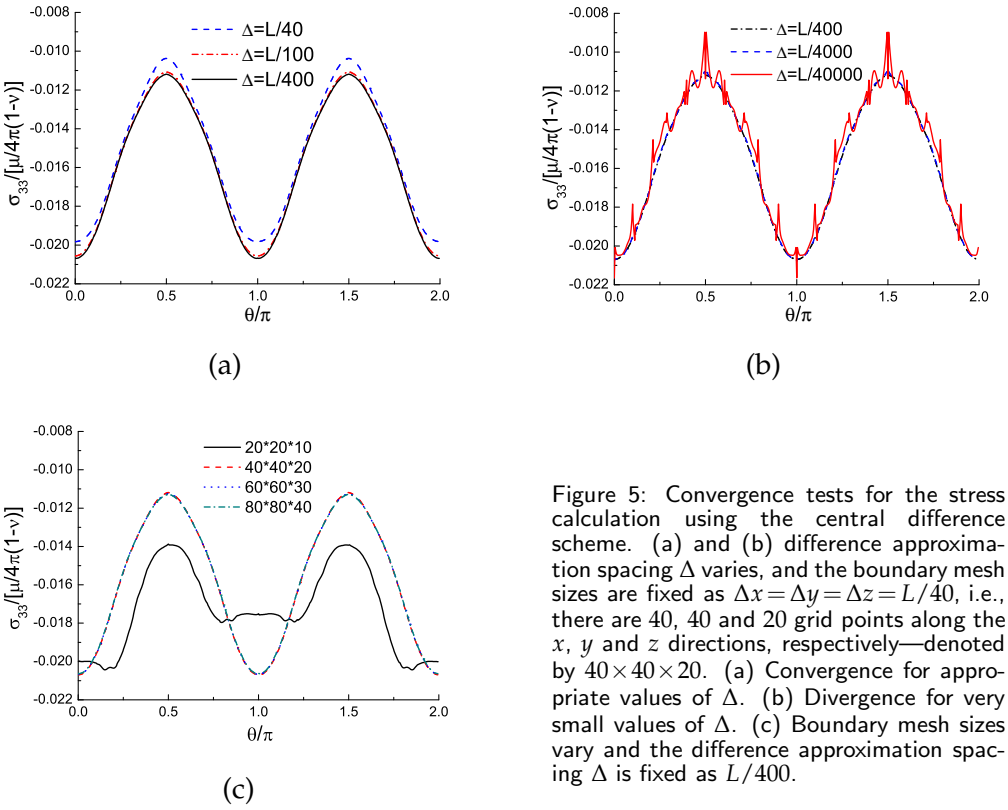

Figure 5: Convergence tests for the stress calculation using the central difference scheme. (a) and (b) difference approximation spacing Δ varies, and the boundary mesh sizes are fixed as $\Delta x=\Delta y=\Delta z=L/40$, i.e., there are 40, 40 and 20 grid points along the x, y and z directions, respectively—denoted by $40\times40\times20$. (a) Convergence for appropriate values of Δ. (b) Divergence for very small values of Δ. (c) Boundary mesh sizes vary and the difference approximation spacing Δ is fixed as $L/400$.

proximations to calculate the stress from the displacement obtained by Eq. (3.5) (see also Eqs. (2.2) and (2.3)). In our calculations, central difference formula is used to approximate the spatial derivatives, using spacing Δ, e.g.,

$$\frac{\partial u_i(x',y',z')}{\partial x}=\frac{u_i(x'+\Delta,y',z')-u_i(x'-\Delta,y',z')}{2\Delta}.$$

The error tolerance is fixed to 10^{-6} in the restarted GMRES solver and the number of expansion terms in the FMM is set to be $p=18$ (so that the relative error is also about 10^{-6} [26]). Note that the accuracy of $\hat{\sigma}_{33}$ is determined by both the boundary mesh size and the choice of Δ when approximating the derivatives using central difference. We choose $\hat{\sigma}_{33}$ on the dislocation loop as an example to investigate the convergence of our numerical method. We first discretize the box boundary using grid sizes $\Delta x=\Delta y=\Delta z=L/40$, i.e., there are 40, 40 and 20 grid points along the x, y and z directions, respectively, and investigate how the results depend on Δ. The results are shown in Fig. 5(a) and (b). We see that when Δ decreases from $L/40$ to $L/400$, the results converge, as shown in Fig. 5(a). However, for smaller Δ, the results diverge due to the instability in the central difference approximation, see Fig. 5(b). This is because when we numerically evaluate $\Delta u/\Delta$, as the error of u is about 10^{-6}, if the magnitude order of Δ decreases to a comparable order of

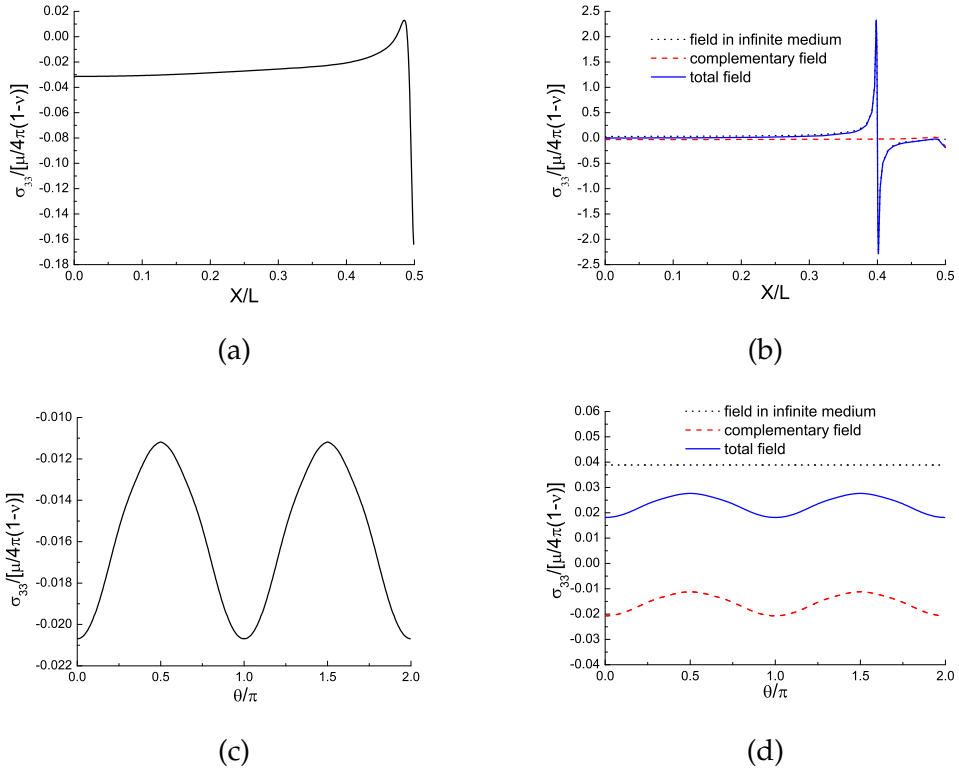

Figure 6: (a) The complementary stress component $\hat{\sigma}_{33}$ of a prismatic dislocation loop placed in a cuboid box. The values along the x axis from the center of the dislocation loop are plotted. (b) The stress components $\hat{\sigma}_{33}$, $\tilde{\sigma}_{33}$, and σ_{33} along the x axis from the center of the dislocation loop. (c) The complementary stress component $\hat{\sigma}_{33}$ on the dislocation loop. (d) The stress components $\hat{\sigma}_{33}$, $\tilde{\sigma}_{33}$ and σ_{33} on the dislocation loop. In (c) and (d), θ is the central angle from x axis in the counterclockwise direction.

10^{-6}, the results will obviously diverge. An alternative approach currently being considered for computing the derivatives is to differentiate the local expansions for the far-field contribution in FMM. However this option will be slower than the difference approximation technique and is less preferred when efficiency is the top priority, such as in dislocation dynamics. In Fig. 5(c), we show the convergence of $\hat{\sigma}_{33}$ with respect to different boundary mesh sizes, with a fixed $\Delta = L/400$. When the boundaries are discretized using 20, 20 and 10 points along x, y and z directions, respectively, i.e., $\Delta x = \Delta y = \Delta z = L/20$, the result is not smooth and the error is large due to the coarse mesh. When smaller mesh sizes are used, we observe convergence.

The obtained results of stress using $\Delta x = \Delta y = \Delta z = L/40$ and $\Delta = L/400$ are summarized in Fig. 6. Fig. 6(a) shows the complementary stress component $\hat{\sigma}_{33}$ along the x axis from the center of the dislocation loop and Fig. 6(b) shows the comparison of $\hat{\sigma}_{33}$ and the stress component in an infinite medium $\tilde{\sigma}_{33}$. The total stress $\sigma_{33} = \hat{\sigma}_{33} + \tilde{\sigma}_{33}$ along the x axis is also presented in Fig. 6(b). It can be seen that away from the boundary, $\hat{\sigma}_{33}$ varies very

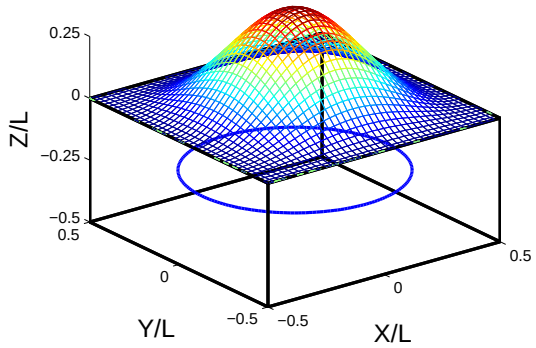

Figure 7: A prismatic dislocation loop in a cuboid box with a curved top surface.

slowly. Whereas when approaching the surface, $\hat{\sigma}_{33}$ varies rapidly. This phenomenon qualitatively agrees with that of the complementary stress field of some straight dislocations where analytical formulas are available [1]. Away from the dislocation loop and box boundary, $\tilde{\sigma}_{33}$ and $\hat{\sigma}_{33}$ are comparable. Near the dislocation loop, $\tilde{\sigma}_{33}$ dominates and when approaching the box boundary, $\hat{\sigma}_{33}$ dominates.

Fig. 6(c) shows the complementary stress component $\hat{\sigma}_{33}$ on the dislocation loop and Fig. 6(d) shows the comparison of $\hat{\sigma}_{33}$ and the stress component in an infinite medium $\tilde{\sigma}_{33}$ and the total field $\sigma_{33}=\hat{\sigma}_{33}+\tilde{\sigma}_{33}$ on the dislocation loop. We can see that $\hat{\sigma}_{33}$ is oscillating along the dislocation loop. When $\theta=0,\pi/2,\pi,3\pi/2$, the absolute value of $\hat{\sigma}_{33}$ reaches maximum, which is related to the fact that these points are closer to the boundary of the box. On the contrary, for the dislocation loop in the infinite medium, the stress component $\tilde{\sigma}_{33}$ is a constant along itself.

In the next example, we make a small perturbation on the top surface of the box, see Fig. 7. The explicit function of the top surface is

$$z(x,y)=0.1L\left(\cos\frac{2\pi}{L}x+1\right)\left(\cos\frac{2\pi}{L}y+1\right).$$

We investigate the influence of the perturbation on the top surface. The parameters are the same as those in the previous example. The complementary stress component $\hat{\sigma}_{33}$ due to the box with flat top surface and curved top surface is presented in Fig. 8. Fig. 8 clearly shows that the absolute value of $\hat{\sigma}_{33}$ of curved top surface is less than that of the flat top surface, which agrees with the fact that the dislocation loop is farther from the curved surface than the original flat one.

Finally, we consider an array of seven circular glide dislocation loops contained in the $L\times L\times L/2$ cuboid box, see Fig. 9(a). The dislocation loops are parallel to the xy plane and the Burgers vector $\mathbf{b}$ is in the x direction. The radius of the dislocation loops is $r=0.4L=200b$ and the distance between adjacent loops is $25b$. Traction-free boundary conditions are used for the whole boundary. Discretization parameters are $\Delta x=\Delta y=\Delta z=L/40$ and $\Delta=L/400$. We calculate the stress component σ_{13} along the center loop and the

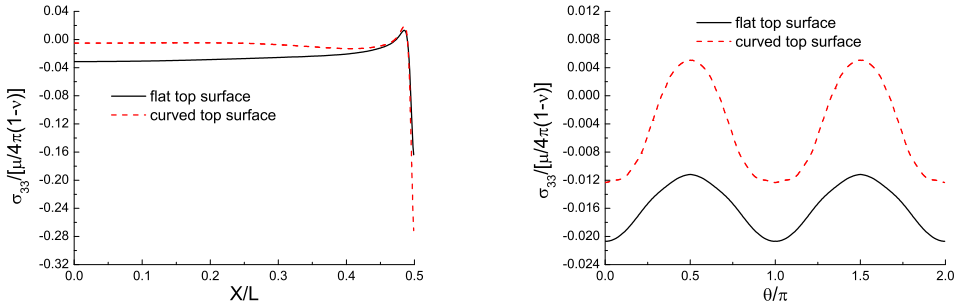

Figure 8: The complementary stress component $\hat{\sigma}_{33}$ for the prismatic dislocation loop in the cuboid box with flat and curved top surfaces. (a) Along x axis from the center of the dislocation loop. (b) On the dislocation loop.

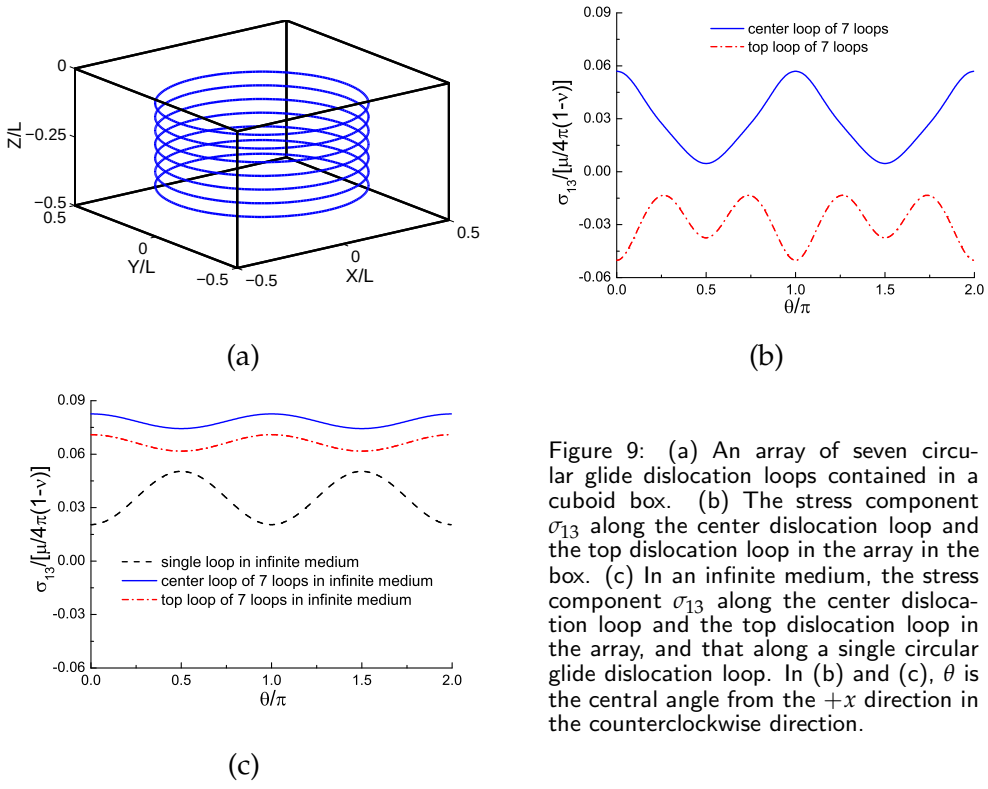

Figure 9: (a) An array of seven circular glide dislocation loops contained in a cuboid box. (b) The stress component σ_{13} along the center dislocation loop and the top dislocation loop in the array in the box. (c) In an infinite medium, the stress component σ_{13} along the center dislocation loop and the top dislocation loop in the array, and that along a single circular glide dislocation loop. In (b) and (c), θ is the central angle from the $+x$ direction in the counterclockwise direction.

top loop, see Fig. 9(b). For the purpose of comparison, the values of σ_{13} along a single dislocation loop, the center loop and the top loop in the array in an infinite medium are also calculated, see Fig. 9(c).

The stress component σ_{13} generates a force in the slip plane of a dislocation loop, which drives the loop to expand or shrink (positive force: shrink; negative force: expand).

For a single loop in an infinite medium, this self-force makes the loop shrink and the driving force has its maximum at the screw points and minimum at the edge points of the loop (see [1], Section 6-5), see the result shown in Fig. 9(c). Due to the long-range interaction of dislocations, the values of this stress component along a dislocation loop in the array are quite different from those along a single dislocation loop, see Fig. 9(c). Comparing the results of dislocation loops in the box in Fig. 9(b) with the corresponding ones in an infinite medium in Fig. 9(c), one can see that the boundaries of the box play the role of attracting the loops, i.e., driving the loops to expand, in contrast with the self-force of dislocation loops in an infinite medium, so that the dislocation loops in the array in the box may either expand or shrink depending on the location of the loops due to the competition between the force due to interaction of dislocations including the dislocation self-force and the force due to material boundaries.

6 Conclusions and discussion

We have developed an efficient numerical method based on the boundary integral equation formulation and new version fast multipole method to solve the boundary value problem for the stress field associated with dislocations in a finite medium. Numerical examples are presented to show the accuracy of the method and investigate the influence of material boundaries on dislocations.

These developed numerical methods and formulations are for dislocations in an isotropic medium. The generalization of our methods and formulations to dislocations in an anisotropic medium is currently being considered. An important application of the developed methods is the dislocation dynamics in thin film materials, which is being studied and results will be presented in the future.

Appendix: Numerical formulation for the singular integrals

The integrals in the boundary integral equations Eq. (3.1) are singular over the boundary element containing the target point itself. In this appendix, we derive numerical approximations to these singular integrals based on linear approximation of the boundary.

We present the formulation for square boundary elements, which are used in this paper. Consider a boundary element S_0 parameterized by $z=z(x,y)$ for $(x,y)\in[-v,v]\times[-v,v]$, see Fig. 10. Let the center of the boundary element be $O=(0,0,z_0)$ and $P=(x,y,z)$ be any point on the element. Using linear approximation, the boundary is

$$z=z_0+x\frac{\partial z}{\partial x}(0,0)+y\frac{\partial z}{\partial y}(0,0),\quad (x,y)\in[-v,v]\times[-v,v]. \tag{A.1}$$

Denote

$$c=\frac{\partial z}{\partial x}(0,0)\quad\text{and}\quad d=\frac{\partial z}{\partial y}(0,0).$$

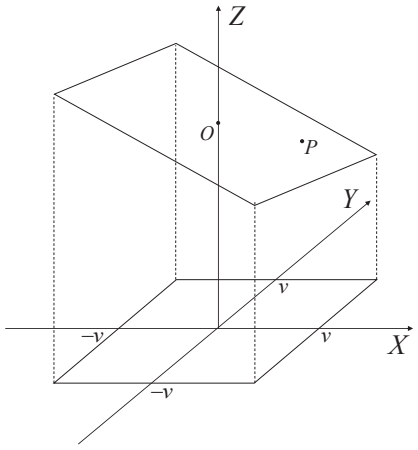

Figure 10: A boundary element S_0 under linear approximation.

Then the distance between points P and O is

$$R=\sqrt{x^2+y^2+(z-z_0)^2}=\sqrt{x^2+y^2+c^2x^2+d^2y^2+2cdxy}, \tag{A.2}$$

and the singular integrals over this boundary element S_0 can be expressed as

$$\int_{S_0} U_{ij}t_j dS=\int_{-v}^{v}dy\int_{-v}^{v}dx U_{ij}(x,y,z)t_j(x,y,z)\sqrt{1+c^2+d^2}, \tag{A.3a}$$

$$\int_{S_0} T_{ij}u_j dS=\int_{-v}^{v}dy\int_{-v}^{v}dx T_{ij}(x,y,z)u_j(x,y,z)\sqrt{1+c^2+d^2}. \tag{A.3b}$$

We also use linear approximation for the traction and displacement in the integrals:

$$t_j(x,y,z)=t_j(0,0,z_0)+\left(x\frac{\partial}{\partial x}+y\frac{\partial}{\partial y}\right)t_j\big|_{(0,0,z_0)}, \tag{A.4a}$$

$$u_j(x,y,z)=u_j(0,0,z_0)+\left(x\frac{\partial}{\partial x}+y\frac{\partial}{\partial y}\right)u_j\big|_{(0,0,z_0)}. \tag{A.4b}$$

The obtained approximation formulas for the singular integrals are

$$\int_{S_0} U_{11}t_1 dS=\frac{t_1(0,0,z_0)}{16\pi\mu(1-\nu)}\sqrt{1+c^2+d^2}[(3-4\nu)p_1+p_2], \tag{A.5a}$$

$$\int_{S_0} U_{22}t_2 dS=\frac{t_2(0,0,z_0)}{16\pi\mu(1-\nu)}\sqrt{1+c^2+d^2}[(3-4\nu)p_1+p_3], \tag{A.5b}$$

$$\int_{S_0} U_{33}t_3 dS=\frac{t_3(0,0,z_0)}{16\pi\mu(1-\nu)}\sqrt{1+c^2+d^2}[(3-4\nu)p_1+c^2p_2+d^2p_3+2cdp_4], \tag{A.5c}$$

$$\int_{S_0} U_{12}t_2 dS = \frac{t_2(0,0,z_0)}{16\pi\mu(1-\nu)}\sqrt{1+c^2+d^2}\,p_4, \tag{A.5d}$$

$$\int_{S_0} U_{13}t_3 dS = \frac{t_3(0,0,z_0)}{16\pi\mu(1-\nu)}\sqrt{1+c^2+d^2}(cp_2+dp_4), \tag{A.5e}$$

$$\int_{S_0} U_{21}t_1 dS = \frac{t_1(0,0,z_0)}{16\pi\mu(1-\nu)}\sqrt{1+c^2+d^2}\,p_4, \tag{A.5f}$$

$$\int_{S_0} U_{23}t_3 dS = \frac{t_3(0,0,z_0)}{16\pi\mu(1-\nu)}\sqrt{1+c^2+d^2}(cp_4+dp_3), \tag{A.5g}$$

$$\int_{S_0} U_{31}t_1 dS = \frac{t_1(0,0,z_0)}{16\pi\mu(1-\nu)}\sqrt{1+c^2+d^2}(cp_2+dp_4), \tag{A.5h}$$

$$\int_{S_0} U_{32}t_2 dS = \frac{t_2(0,0,z_0)}{16\pi\mu(1-\nu)}\sqrt{1+c^2+d^2}(cp_4+dp_3), \tag{A.5i}$$

$$\int_{S_0} T_{11}u_1 dS = \int_{S_0} T_{22}u_2 dS = \int_{S_0} T_{33}u_3 dS = 0, \tag{A.5j}$$

$$\int_{S_0} T_{12}u_2 dS = \frac{1-2\nu}{8\pi(1-\nu)}\Big(-dp_2\frac{\partial}{\partial x} - dp_4\frac{\partial}{\partial y} + cp_4\frac{\partial}{\partial x} + cp_3\frac{\partial}{\partial y}\Big)u_2(0,0,z_0), \tag{A.5k}$$

$$\int_{S_0} T_{13}u_3 dS = \frac{1-2\nu}{8\pi(1-\nu)}\Big[(p_2+c^2p_2+cdp_4)\frac{\partial}{\partial x} + (n_3p_4+c^2p_4+cdp_3)\frac{\partial}{\partial y}\Big]u_3(0,0,z_0), \tag{A.5l}$$

$$\int_{S_0} T_{21}u_1 dS = \frac{1-2\nu}{8\pi(1-\nu)}\Big(-cp_4\frac{\partial}{\partial x} - cp_3\frac{\partial}{\partial y} + dp_2\frac{\partial}{\partial x} + dp_4\frac{\partial}{\partial y}\Big)u_1(0,0,z_0), \tag{A.5m}$$

$$\int_{S_0} T_{23}u_3 dS = \frac{1-2\nu}{8\pi(1-\nu)}\Big[(p_4+cdp_2+d^2p_4)\frac{\partial}{\partial x} + (p_3+cdp_4+d^2p_3)\frac{\partial}{\partial y}\Big]u_3(0,0,z_0), \tag{A.5n}$$

$$\int_{S_0} T_{31}u_1 dS = \frac{1-2\nu}{8\pi(1-\nu)}\Big[(-c^2p_2-cdp_4-p_2)\frac{\partial}{\partial x} + (-c^2p_4-cdp_3-p_4)\frac{\partial}{\partial y}\Big]u_1(0,0,z_0), \tag{A.5o}$$

$$\int_{S_0} T_{32}u_2 dS = \frac{1-2\nu}{8\pi(1-\nu)}\Big[(-cdp_2-d^2p_4-p_4)\frac{\partial}{\partial x} + (-cdp_4-d^2p_3-p_3)\frac{\partial}{\partial y}\Big]u_2(0,0,z_0), \tag{A.5p}$$

where

$$\begin{aligned} p_1 &= \int_{-v}^{v}dy\int_{-v}^{v}dx\frac{1}{\sqrt{x^2+y^2+c^2x^2+d^2y^2+2cdxy}} \\ &= \frac{2v}{\sqrt{1+d^2}}\ln\frac{1+d^2+cd+\sqrt{(1+d^2)(2+c^2+d^2+2cd)}}{cd+\sqrt{(1+c^2)(1+d^2)}} \\ &\quad + \frac{2v}{\sqrt{1+c^2}}\ln\frac{1+c^2+cd+\sqrt{(1+c^2)(2+c^2+d^2+2cd)}}{cd+\sqrt{(1+c^2)(1+d^2)}} \\ &\quad + \frac{2v}{\sqrt{1+d^2}}\ln\frac{1+d^2-cd+\sqrt{(1+d^2)(2+c^2+d^2+2cd)}}{-cd+\sqrt{(1+c^2)(1+d^2)}} \\ &\quad + \frac{2v}{\sqrt{1+c^2}}\ln\frac{1+c^2-cd+\sqrt{(1+c^2)(2+c^2+d^2+2cd)}}{-cd+\sqrt{(1+c^2)(1+d^2)}}, \end{aligned} \tag{A.6a}$$

$$
\begin{aligned}
p_2 &= \int_{-v}^{v} dy \int_{-v}^{v} dx \frac{x^2}{(x^2+y^2+c^2x^2+d^2y^2+2cdxy)^{3/2}} \\
&= 2cdv \frac{\sqrt{2+c^2+d^2+2cd}-\sqrt{2+c^2+d^2-2cd}}{(1+c^2)(1+c^2+d^2)} \\
&\quad + \frac{2v}{(1+c^2)^{3/2}} \ln \frac{1+c^2+cd+\sqrt{(1+c^2)(2+c^2+d^2+2cd)}}{cd+\sqrt{(1+c^2)(1+d^2)}} \\
&\quad + \frac{2v}{(1+c^2)^{3/2}} \ln \frac{1+c^2-cd+\sqrt{(1+c^2)(2+c^2+d^2+2cd)}}{-cd+\sqrt{(1+c^2)(1+d^2)}}, \qquad \text{(A.6b)} \\
p_3 &= \int_{-v}^{v} dy \int_{-v}^{v} dx \frac{y^2}{(x^2+y^2+c^2x^2+d^2y^2+2cdxy)^{3/2}} \\
&= 2cdv \frac{\sqrt{2+c^2+d^2+2cd}-\sqrt{2+c^2+d^2-2cd}}{(1+d^2)(1+c^2+d^2)} \\
&\quad + \frac{2v}{(1+d^2)^{3/2}} \ln \frac{1+d^2+cd+\sqrt{(1+d^2)(2+c^2+d^2+2cd)}}{cd+\sqrt{(1+c^2)(1+d^2)}} \\
&\quad + \frac{2v}{(1+d^2)^{3/2}} \ln \frac{1+d^2-cd+\sqrt{(1+d^2)(2+c^2+d^2+2cd)}}{-cd+\sqrt{(1+c^2)(1+d^2)}}, \qquad \text{(A.6c)} \\
p_4 &= \int_{-v}^{v} dy \int_{-v}^{v} dx \frac{xy}{(x^2+y^2+c^2x^2+d^2y^2+2cdxy)^{3/2}} \\
&= \frac{2v}{1+c^2+d^2} \left(\sqrt{2+c^2+d^2-2cd}-\sqrt{2+c^2+d^2+2cd} \right). \qquad \text{(A.6d)}
\end{aligned}
$$

Note that in these formulas, the partial derivatives of u_j and t_j with respect to x and y can be approximated numerically by finite difference expressions.

Acknowledgments

This work is partially supported by Hong Kong Research Grants Council General Research Fund 604208 and the Nano Science and Technology Program at HKUST.

References

[1] J. P. Hirth and J. Lothe, Theory of Dislocations, 2nd ed., John Wiley, New York, 1982.
[2] A. N. Gullouglu, D. J. Srolovitz, R. LeSar and P. S. Lomdahl, Dislocation distributions in two dimensions, Scripta Metall., 23 (1989), 1347–1352.
[3] L. P. Kubin, G. Canova, M. Condat, B. Devincre, V. Pontikis and Y. Brechet, Dislocation microstructures and plastic flow: a 3D simulation, Solid State Phenom., 23/24 (1992), 455–472.
[4] H. Y. Wang and R. LeSar, $\mathcal{O}(N)$ algorithm for dislocation dynamics, Phil. Mag. A, 71 (1995), 149–164.

[5] M. C. Fivel, T. J. Gosling and G. R. Canova, Implementing image stresses in a 3D dislocation simulations, Model. Simul. Mater. Sci. Eng., 4 (1996), 581–596.
[6] H. M. Zbib, M. Rhee and J. P. Hirth, On plastic deformation and the dynamics of 3D dislocations, Int. J. Mech. Sci., 40 (1998), 113–127.
[7] M. Verdier, M. Fivel and I. Groma, Mesoscopic scale simulation of dislocation dynamics in FCC metals: principles and applications, Model. Simul. Mater. Sci. Eng., 6 (1998), 755–770.
[8] K. W. Schwarz, Simulation of dislocations on the mesoscopic scale I: methods and examples, J. Appl. Phys., 85 (1999), 108–119.
[9] N. M. Ghoniem, S. H. Tong and L. Z. Sun, Parametric dislocation dynamics: a thermodynamics-based approach to investgations of mesoscopic plastic deformation, Phys. Rev. B, 61 (2000), 913–927.
[10] D. Weygand, L. H. Friedman, E. Van der Giessen and A. Needleman, Aspects of boundary-value problem solutions with three-dimensional dislocation dynamics, Model. Simul. Mater. Sci. Eng., 10 (2002), 437–468.
[11] R. LeSar and J. M. Rickman, Multipole expansion of dislocation interactions: application to discrete dislocations, Phys. Rev. B, 65 (2002), 144110.
[12] R. Martinez and N. M. Ghoniem, The influence of crystal surfaces on dislocation interactions in mesoscopic plasticity: a combined dislocation dynamics-finite element approach, Comput. Model. Eng. Sci., 3 (2002), 229–245.
[13] T. A. Khraishi and H. M. Zbib, Free-surface effects in 3D dislocation dynamics: formulation and modelling, J. Eng. Mat. Tech., 124 (2002), 342–351.
[14] S. Groh, B. Devincre, L. P. Kubin, A. Roos, F. Feyel and J. L. Chaboche, Dislocation and elastic anisotropy in heteroepitaxial metallic thin films, Phil. Mag. Lett., 83 (2003), 303–313.
[15] Y. Xiang, L. T. Cheng, D. J. Srolovitz and W. E, A level set method for dislocation dynamics, Acta Mater., 51 (2003), 5499–5518.
[16] L. Yan, T. A. Khraishi, Y. L. Shen and M. F. Horstemeyer, A distributed dislocation method for treating free-surface image stresses in three dimensional dislocation dynamics simulations, Model. Simul. Mater. Sci. Eng., 12 (2004), S289–S301.
[17] Z. Wang, N. M. Ghoniem and R. LeSar, Multipole representation of the elastic field of dislocation ensembles, Phys. Rev. B, 69 (2004), 174102.
[18] X. H. Liu and K. W. Schwarz, Modelling of dislocation intersecting a free surface, Model. Simul. Mater. Sci. Eng., 13 (2005), 1233–1247.
[19] S. S. Quek, Y. Xiang, Y. W. Zhang, D. J. Srolovitz and C. Lu, Level set simulation of dislocation dynamics in thin films, Acta Mater., 54 (2006), 2371–2381.
[20] Y. Xiang, Modeling dislocations at different scales, Commun. Comput. Phys., 1 (2006), 383–424.
[21] Z. Wang, N. M. Ghoniem, S. Swaminarayan and R. LeSar, A parallel algorithm for 3D dislocation dynamics, J. Comput. Phys., 219 (2006), 608–621.
[22] M. J. Tang, W. Cai, G. S. Xu and V. V. Bulatov, A hybrid method for computing forces on curved dislocations intersecting free surfaces in three-dimensional dislocation dynamics, Model. Simul. Mater. Sci. Eng., 14 (2006), 1139–1151.
[23] A. Arsenlis, W. Cai, M. Tang, M. Rhee, T. Oppelstrup, G. Hommes, T. G. Pierce and V. V. Bulatov, Enabling strain hardening simulations with dislocation dynamics, Model. Simul. Mater. Sci. Eng., 15 (2007), 553–595.
[24] J. A. El-Awady, S. B. Biner and N. M. Ghoniem, A self-consistent boundary element, parametric dislocation dynamics formulation of plastic flow in finite volumes, J. Mech. Phys. Solids, 56 (2008), 2019–2035.

[25] S. S. Quek, Y. W. Zhang, Y. Xiang and D. J. Srolovitz, Dislocation cross-slip in heteroepitaxial multilayer films, Acta Mater., 58 (2010), 226–234.
[26] D. G. Zhao, J. F. Huang and Y. Xiang, A new version fast multipole method for evaluating the stress field of dislocation ensembles, Model. Simul. Mater. Sci. Eng., 18 (2010), 045006.
[27] L. Greengard and V. Rokhlin, A new version of the fast multipole method for the Laplace equation in three dimensions, Acta Numer., 6 (1997), 229–269.
[28] E. Van der Giessen and A. Needleman, Discrete dislocation plasticity: a simple planar model, Model. Simul. Mater. Sci. Eng., 3 (1995), 689–735.
[29] C. A. Brebbia, The Boundary Element Method for Engineers, Pentech Press, London, 1978.
[30] Y. Fu, K. J. Klimkowski, G. J. Rodin, E. Berger, J. C. Browne, J. K. Singer, R. A. Van De Geijn and K. S. Vemaganti, A fast solution method for three-dimensional many-particle problems of linear elasticity, Int. J. Numer. Meth. Eng., 42 (1998), 1215–1229.
[31] Y. Fu and G. J. Rodin, Fast solution method for three-dimensional Stokesian many-particle problems, Commun. Numer. Meth. Eng., 16 (2000), 145–149.
[32] K. Yoshida, N. Nishimura and S. Kobayashi, Application of new fast multipole boundary integral equation method to elastostatic crack problems, J. Struct. Eng., 47A (2001), 169–179.
[33] N. Nishimura, Fast multipole accelerated boundary integral equation methods, Appl. Mech. Rev., 55 (2000), 299–324.
[34] Y. S. Lai and G. J. Rodin, Fast boundary element method for three-dimensional solids containing many cracks, Eng. Anal. Bound. Elem., 27 (2003), 845–852.
[35] H. Wang, T. Lei, J. Li, J. F. Huang and Z. Yao, A parallel fast multipole accelerated integral equation scheme for 3D Stokes equations, Int. J. Numer. Meth. Eng., 70 (2007), 812–839.
[36] Y. Liu, Fast Multipole Boundary Element Method: Theory and Applications in Engineering, Cambridge University Press, New York, 2009.
[37] M. Peach and J. S. Koehler, The forces exerted on dislocations and the stress fields produced by them, Phys. Rev., 80 (1950), 436–439.
[38] R. Barrett, M. Berry, T. F. Chan, J. Demmel, J. M. Donato, J. Dongarra, V. Eijkhout, R. Pozo, C. Romine and H. Van der Vorst, Templates for the Solution of Linear Systems: Building Blocks for Iterative Methods, 2nd Ed., SIAM, Philadelphia, 1994.
[39] J. A. Bettess, Economical solution technique for boundary integral matrices, Int. J. Numer. Meth. Eng., 19 (1983), 1073–1077.
[40] Y. Saad and M. H. Schultz, GMRES: a generalized minimum residual algurithm for solving nonsymmetric linear systems, SIAM J. Sci. Stat. Comput., 7 (1986), 856–869.
[41] R. L. Mullen and J. J. Rencis, Iterative methods for solving boundary element equations, Comput. Struct., 25 (1987), 713–723.
[42] N. Phan-Thien and S. Kim, Microstructure in Elastic Media: Principles and Computational Methods, Oxford University, New York, 1994.
[43] F. P. Valente and H. L. Pina, Iterative techniques for 3-D boundary element method systems of equations, Eng. Anal. Bound. Elem., 25 (2001), 423–429.
[44] `http://fastmultipole.org/`.
[45] J. Huang, J. Jia and B. Zhang, FMM-Yukawa: an adaptive fast multipole method for screened Coulomb interactions, Comput. Phys. Commun., 180 (2009), 2331–2338.
[46] A. Pimpinelli and J. Villain, Physics of Crystal Growth, Cambridge University Press, New York, 1998.